Check for updates

Received: 31 March 2019 | Revised and accepted: 8 April 2019

DOI: 10.1002/inf2.12006

ORIGINAL ARTICLE

WILEY

Ultrahigh figure-of-merit of Cu_2Se incorporated with carbon coated boron nanoparticles

Meng Li[1] | **Sheik Md. Kazi Nazrul Islam**[1] | **Mujde Yahyaoglu**[2] | **Deng Pan**[3] | **Xun Shi**[4] | **Lidong Chen**[4] | **Umut Aydemir**[5,6] | **Xiaolin Wang**[1,7]

[1]Institute for Superconducting and Electronic Materials, Australian Institute for Innovative Materials, University of Wollongong, North Wollongong, NSW, Australia

[2]Graduate School of Sciences and Engineering, Koç University, Sariyer, Istanbul, Turkey

[3]Shandong YiAn Bio-Engineering Co., Ltd., Jinan, Shandong, China

[4]State Key Laboratory of High Performance Ceramics and Superfine Microstructures, Shanghai Institute of Ceramics, Chinese Academy of Sciences, Shanghai, P. R. China

[5]Department of Chemistry, Koç University, Sariyer, Istanbul, Turkey

[6]Koç University Akkim Boron-Based Materials and High Technology Chemicals Research and Application Center, Sariyer, Istanbul, Turkey

[7]ARC Centre of Excellence in Future Low-Energy Electronics Technologies, University of Wollongong, Australia

Correspondence
Xiaolin Wang, University of Wollongong, Wollongong, NSW, Australia.
Email: xiaolin@uow.edu.au

Funding information
Australian Research Council, Grant/Award Numbers: DP 130102956, FT 130100778; Linkage Infrastructure Equipment and Facilities, Grant/Award Numbers: LE 120100069, CE170100039

Abstract

Cu_2Se based thermoelectric materials are of great potential for high-temperature energy harvesting due to their high-temperature figure-of-merit (zT). For further development of Cu_2Se, both engineering and mid-temperature figure-of-merit need to be improved. In this work, we report that carbon-coated boron (C/B) nanoparticles incorporation can significantly improve both mid- and high-temperature zT in Cu_2Se. The nanoparticle inclusions can result in a homogeneous distribution of Cu:C:B interfaces responsible for both improvement of the Seebeck coefficient and significantly reduction in thermal conductivity. Ultrahigh mid- and high temperature thermoelectric performance with $zT = 1.7$ at 700 K and 2.23 at 1000 K as well as significantly improved engineering zT are achieved in the C/B incorporated Cu_2Se with desirable mechanical properties and cycling stability. Our findings will stimulate further study and exploration for the Cu_2Se based thermoelectric materials for broad applications in converting waste heat to electricity with competitive energy conversion efficiency.

KEYWORDS

average/engineering zT, mid-temperature zT, nanoparticle incorporation, thermoelectric

1 | INTRODUCTION

Improving energy conversion efficiency in thermoelectric (TE) materials can greatly enhances their prospects for extensive commercial applications.[1-3] As an evaluation for energy conversion efficiency, figure-of-merit (zT) is the decisive factor to screen good TE materials, namely $zT = S^2\sigma T/\kappa$, where S, σ, T, and κ are the Seebeck coefficient, electrical conductivity, absolute temperature in Kelvin, and thermal conductivity, respectively.[4-7] In the past decades, many novel concepts and

This is an open access article under the terms of the Creative Commons Attribution License, which permits use, distribution and reproduction in any medium, provided the original work is properly cited.
© 2019 The Authors. *InfoMat* published by John Wiley & Sons Australia, Ltd on behalf of UESTC.

effective experimental approaches aiming to enhance zT have emerged, such as band convergence,[8] phonon-glass electron-crystal,[9] multiscale phonon scattering,[10] resonant states,[11] anharmonicity,[12] quantum confinement,[13] and grain boundary engineering,[8] and so on. Consequently, these methods have been adopted to successfully raise up the zTs in a wide range of TE materials, including SnSe, PbTe, GeTe, $CoSb_3$, Bi-Te, Sb-Te, and so on, promoting TE modules applied in converting waste heat to electricity with competitive energy conversion efficiency.[14-19]

The value of zT could be enhanced via increasing the power factor ($PF = S^2\sigma$) or decreasing the thermal conductivity ($\kappa = \kappa_L + \kappa_C$), where κ_L and κ_C are the lattice and charge carrier thermal conductivity, respectively.[20-22] However, S and σ usually couple together limiting the modulation of PF, thus the lattice thermal conductivity that solely depends upon on phonon propagation is often considered to be the vital factor for maximizing zT.[23-26] Besides the maximum zT, the efficiency of TE modules also depends on the material's average zT (zT_{avg}) and engineering zT (zT_{eng}).[27-29] Therefore, it is imperative to raise both the zT_{avg} and zT_{eng} over the whole temperature range for device's operation application. Great efforts have been devoted to enhancing the zT_{avg} and zT_{eng} through tuning charge carrier scattering mechanism,[30] band structure engineering,[31] or hierarchical architectures.[32] The key objective of these strategies is to enhance the mid-temperature zT, and form a "plateau" that persists to high-temperature.[2,33]

Recently, carbon incorporated Cu_2Se has been reported to reach an ultrahigh figure-of-merit (zT ~2.4) due to drastically suppressed lattice thermal conductivity.[34,35] However, the mid-temperature zT and average/engineering zT remain inferior. In this work, we aim to enhance both zT_{avg} and zT_{eng} in Cu_2Se via the incorporation of carbon-coated-boron nanoparticles (C/B-NPs). Boron is proposed a promising secondary phase introduced to TE matrix because of its small atomic number, high melting point, and great chemical stability. Furthermore, the totally different phonon density-of-states (DOS) of boron from Cu_2Se could make boron nanoparticles extra phonon scattering centers. To incorporate more fraction of C/B-NPs in Cu_2Se via eutectic transformation process and increase the coherence between inclusions and the Cu_2Se matrix, carbon buffer layer having similar lattice parameter with high-temperature phase Cu_2Se (as is shown in Figure S1) are introduced. As a result, the C/B-NP incorporated Cu_2Se shows generally increased Seebeck coefficient and decreased thermal conductivity. Maximum zT of ~2.23 at 1000 K is achieved in Cu_2Se incorporated with 0.10% C/B-NPs, and the corresponding zT_{avg} and zT_{eng} are enhanced by 100%. Our work reveals that the C/B-NP incorporated Cu_2Se has great potential for mid-temperature TE applications.

2 | RESULTS AND DISCUSSIONS

A schematic illustration of the sample synthesis via eutectic transformation is shown in Figure 1A. During the melting process, the C/B-NPs disperse in molten Cu_2Se homogeneously. When the temperature cools down, the eutectic phase begins to solidify and the Cu_2Se nucleates on the surfaces of the C/B-NPs. Owing to the similar lattice parameter between C and Cu_2Se, the Cu atoms tend to interact with C atoms and form the Cu:C:B interfaces, causing energy filtering effect which can enhance the Seebeck coefficient, especially when the interfacial barrier potential is similar to that of the Fermi level of the compound.[13,36] For the heat transport, the phonons will be greatly scattered when they pass through the Cu:C and C:B interfaces due to the significant mismatch of the phonon DOS and softened chemical interaction. As a result, the phonon mean-free-

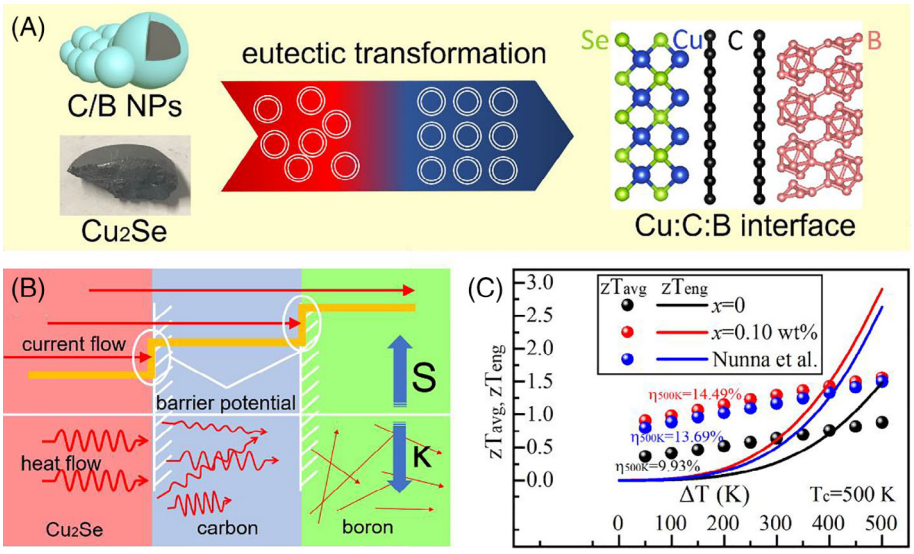


FIGURE 1 Schematic diagram of A, the eutectic transformation synthesis and Cu:C:B interfaces and B, the illustration of energy filter effect and phonon scattering. C, The average figure-of-merit and engineering figure-of-merit in this work and a reported Cu_2Se-based hybrid system[35]

25673165, 2019, 1, Downloaded from https://onlinelibrary.wiley.com/doi/10.1002/inf2.12006 by Koc University, Wiley Online Library on [25/10/2026]. See the Terms and Conditions (https://onlinelibrary.wiley.com/terms-and-conditions) on Wiley Online Library for rules of use; OA articles are governed by the applicable Creative Commons License

path is suppressed, and the thermal conductivity is decreased. This synergistic modulation of the Seebeck coefficient and thermal conductivity should be beneficial for the TE performance, as shown in Figure 1C. The average zT (zT_{avg}) and engineering zT (zT_{eng}) are calculated using the following equations,

$$zT_{avg} = \int_{500\,K}^{1000\,K} zT(T)dT \quad (1)$$

$$zT_{eng} = \frac{\left(\int S(T)dT\right)^2 \cdot \int \sigma(T)dT}{\int \kappa(T)dT} \quad (2)$$

for the C/B-NPs incorporated Cu_2Se and the previously reported carbon nanotube reinforced Cu_2Se.[35] The results show that the zT_{avg} of the sample with 0.10 wt% C/B-NPs is larger than that of the pristine Cu_2Se due to the very high zT values over a broad range of temperature. Accordingly, the $x = 0.10$ wt% sample also shows the highest zT_{eng} of ~2.9 when the temperature difference between the cold side and hot side of a TE module is 500 K. This value is almost twice as high as that in the pristine Cu_2Se, implying that the C/B-NPs incorporation can lead to an ultrahigh energy conversion efficiency at high-temperature ($\eta = 14.49\%$ when $\Delta T = 500$ K).

Figure 2 shows the microscopic characterization of the 0.10 wt% C/B-NPs incorporated Cu_2Se sample. As is shown in Figure 2A, the fractography consists of highly dense compressed Cu_2Se particles in size of ~40 μm, and no preferential orientation is observed. The back-scattered electron (BSE) image and electron backscatter diffraction (EBSD) patterns illustrated in Figure 2B,C, respectively, were acquired from a Ga^+ ion-beam milled surface. It can be seen that incorporated Cu_2Se consists of grains in hierarchical sizes scoping from nanometers to micrometers. The nanometric grains are proposed to be nucleated from C/B-NPs hetero-surface, while the much larger grains should be the agglomeration of Cu_2Se during melting process. Meanwhile, large density of twins are observed as presented in Figure 2C, which could scatter the phonons to reduce thermal conductivity.[37,38]

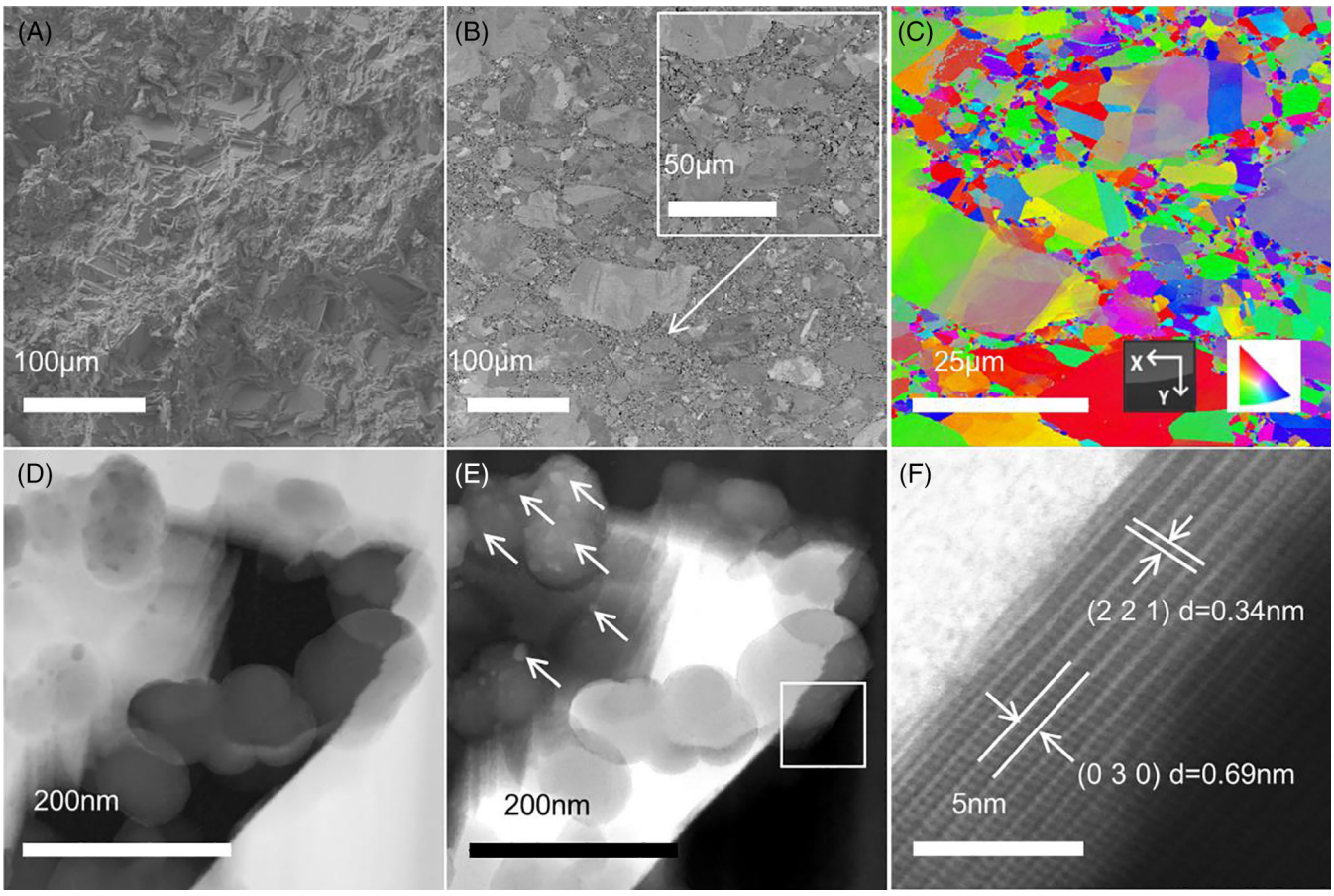


FIGURE 2 A, Scanning electron microscope (SEM) image of the cross-section of the Cu_2Se incorporated with 0.10 wt% carbon-coated-boron nanoparticles. B, BSE image with enlargement shown in inset. C, EBSD pattern for the $x = 0.10$ wt% sample. D, HAADF and E, BF TEM images for the grain boundary region. F, High resolution TEM (HRTEM) image of the labelled area in E, shows the interface between the C/B-NPs and the Cu_2Se matrix. BF TEM, bright field transmission electron microscope; BSE, back-scattered electron; EBSD, electron backscatter diffraction; HAADF, high-angle annular dark field

25673165, 2019, 1, Downloaded from https://onlinelibrary.wiley.com/doi/10.1002/inf2.12006 by Koc University, Wiley Online Library on [25/10/2026]. See the Terms and Conditions (https://onlinelibrary.wiley.com/terms-and-conditions) on Wiley Online Library for rules of use; OA articles are governed by the applicable Creative Commons License

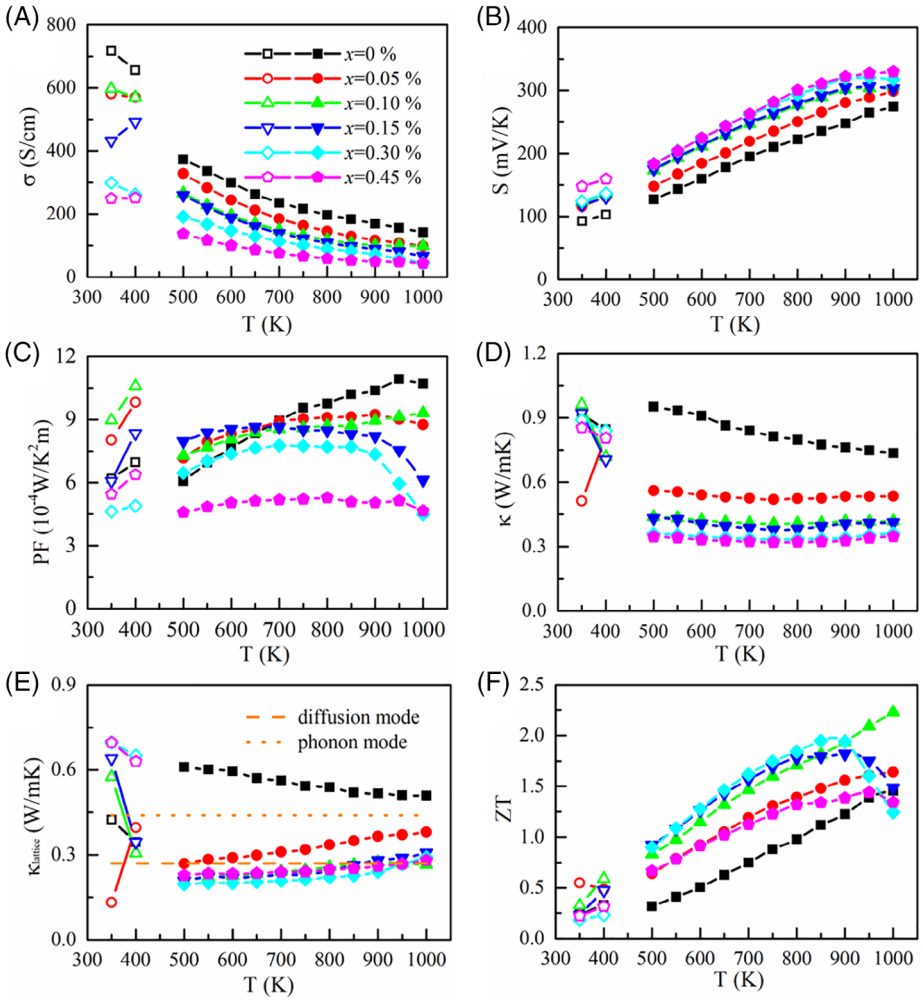


FIGURE 3 Temperature dependence of A, electrical conductivity (σ), B, Seebeck coefficient (S), C, power factor (PF), D, total thermal conductivity (κ), E, lattice thermal conductivity ($\kappa_{lattice}$), and F, figure-of-merit (zT) for pristine and C/B-NPs incorporated Cu_2Se

Figure 2D,E show the high-angle annular dark field (HAADF) and bright field (BF) transmission electron microscope (TEM) images, respectively, for a lamella prepared by the focused ion beam (FIB) cutting. The spherical C/B-NPs in a diameter of ~100 nm are embedded both at grain boundaries and inside the Cu_2Se grains. Some copper-rich areas could be found on the surfaces of C/B-NPs, which are similar to the case reported in carbon incorporated Cu_2Se, indicating that the copper atoms interact with carbon during the melting process at high temperature.[35,39] High-resolution image for the interface between Cu_2Se and C/B-NPs is presented in Figure 2F, where the C/B-NPs appear to be amorphous and compacted by the Cu_2Se matrix, and no visible changes of the d-space of Cu_2Se lattice is detected nearby the interface.

The temperature dependence of electrical conductivity (σ) and Seebeck coefficient (S) is presented in Figure 3A,B, respectively. The σ is reduced from 385 S/cm for $x = 0.05$ wt% to 176 S/cm for $x = 0.45$ wt% at 500 K, and it is reduced from 101 S/cm for $x = 0.05$ wt% to 49 S/cm for $x = 0.45$ wt% at 1000 K. The overall decrease of σ indicates the negative effect induced by C/B-NPs, which is attributed to the following two reasons. One is that the intrinsic low conductivity of boron will reduce the effective electrical conductivity of the system, the other is the Cu:C:B interfaces might induce extra surface states scattering charge carriers and suppressing their mobility. Along with the reduced electrical conductivity, obvious enhancement of S in Cu_2Se with C/B-NPs incorporation is observed for both α- and β-phase. The S of the $x = 0.05$ wt% sample reaches a maximum value of 337 μV/K at 950 K, which is ~137% of pristine Cu_2Se sample. This remarkable enhancement of the Seebeck coefficient should be attributed to the aforementioned energy filter effect derived from the local heterostructures formed by C/B-NPs. Figure 3C presents the temperature dependence of the power factor (PF) in samples with or without C/B-NPs. Unlike the pristine Cu_2Se, the PF of the C/B-NPs incorporated samples do not change much with temperature. For T<700 K, the PF values for the 0.05 wt%< x <0.30 wt% samples are all larger than for the pristine Cu_2Se. While for T>700 K, they show lower values compared with pristine Cu_2Se.

The temperature dependence of the total thermal conductivity (κ) and the calculated lattice thermal conductivity ($\kappa_{lattice}$)

25673165, 2019, 1, Downloaded from https://onlinelibrary.wiley.com/doi/10.1002/inf2.12006 by Koc University, Wiley Online Library on [25/10/2026]. See the Terms and Conditions (https://onlinelibrary.wiley.com/terms-and-conditions) on Wiley Online Library for rules of use; OA articles are governed by the applicable Creative Commons License

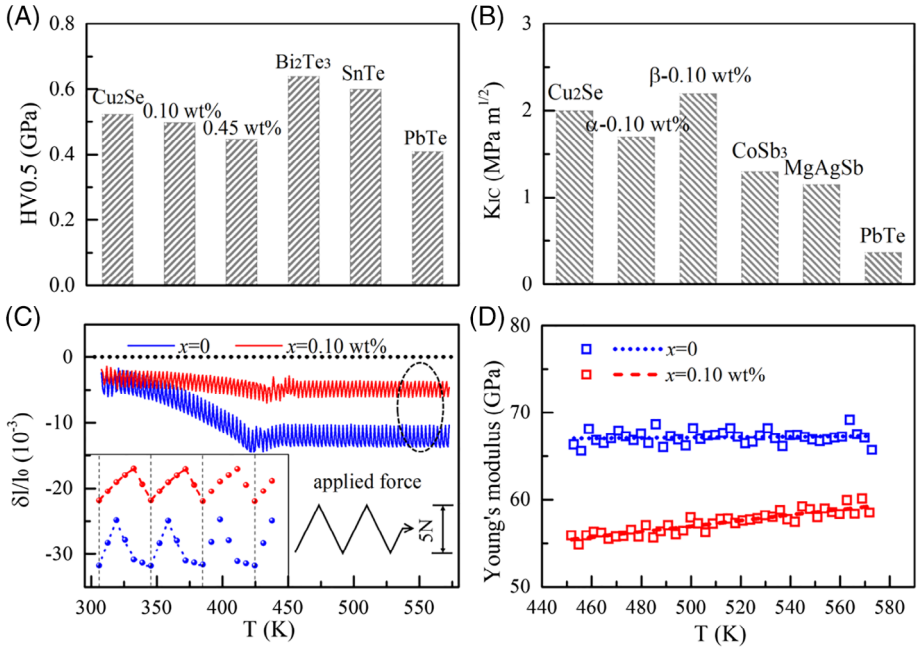


FIGURE 4 A, Vicker's hardness (HV 0.5) and B, fracture toughness (K_{IC}) of fabricated samples in comparison with other traditional thermoelectric materials. C, Bending test for samples with or without carbon-coated-boron nanoparticles; the inset is an enlargement of the labelled area. D, Temperature dependent variation of Young's modulus of fabricated samples

are presented in Figure 3D,E, respectively. The κ of the C/B-NPs incorporated samples is much lower than the pristine Cu_2Se and show an anomalous temperature dependent tendency; it first decreases for $T < 750$ and then increases for $T > 750$ K. Remarkably, the κ decreases from 0.98 W/mK for $x = 0$ to 0.59 W/mK for $x = 0.05$ wt% at 500 K, and it then further decreases to 0.41 W/mK for $x = 0.45$ wt% Cu_2Se. We calculated the lattice thermal conductivity for all samples by subtracting the electronic thermal conductivity from the total thermal conductivity ($\kappa_{lattice} = \kappa_{total} - \kappa_{electron}$). The $\kappa_{electron}$ is calculated based on the Wiedemann-Franz law, namely $\kappa_{electron} = L\sigma T$, where L is the Lorenz number and calculated by $L = 1.5 + \exp\left[-\frac{|S|}{116}\right]$.[40] As is shown in Figure 3E, the C/B-NPs incorporated samples show significantly reduced lattice thermal conductivity, which is even lower than the theoretical prediction based on the diffusion mode of phonon propagation. Interestingly, all the incorporated samples show upward lattice thermal conductivity on increasing temperature. If we treat heat transport as solely mediated by phonons, the lattice thermal conductivity of an isotropic bulk material can be described as[41,42]

$$\kappa_{lattice} = \frac{1}{3} C_v v l \tag{3}$$

where C_v, v, and l are the volumetric heat capacity, the group velocity and mean free path of phonons, respectively. With elevating temperature, both C_v and l should keep constant as the Cu_2Se lattice structure keeps stable up to 1000 K. Nevertheless, v is proposed to be enhanced due to the strengthened chemical interactions between matrix and inclusion, thus increasing $\kappa_{lattice}$.[43-45] From macroscopic view, because

$$\bar{v} = \left[\frac{1}{3}\left(\frac{1}{v_l^3} + \frac{2}{v_s^3}\right)\right]^{-1/3} \tag{4}$$

$$\bar{v} \propto (E/\rho)^{1/2} \tag{5}$$

where $\bar{v}$, v_l, v_s, and E are average phonon velocity, longitudinal phonon velocity, shear phonon velocity, and Young's modulus, respectively.[46-48] For samples with C/B-NPs incorporation, the defects and interfaces will be strongly suppressed at high-temperature due to the different thermal expansion between Cu_2Se and C/B-NPs. Accordingly, the Young's modulus will be enhanced, resulting in an increased $\bar{v}$ and higher $\kappa_{lattice}$.

Figure 3F shows the temperature dependence of the figure-of-merit (zT) in samples with or without incorporated C/B-NPs. All the incorporated samples show appearant enhancement of zT compared with pure Cu_2Se. The overall zTs first increase for the $x = 0.05$ wt% and 0.10 wt% samples, and then decrease for x>0.10 wt% samples. Remarkably, zT of ~1.7 at 700 K is achieved in sample $x = 0.30$ wt %, which is the highest value reported for Cu_2Se in mid-temperature to the best of our knowledge. This implies that the incorporated Cu_2Se has great potential for mid-temperature TE applications. For T>700 K, by combining the ultralow κ and enhanced S, a maximum zT of ~2.23 at 1000 K is eventually achieved for the $x = 0.10$ wt% sample, which is almost 55% higher than the zT of pristine Cu_2Se.

As the TE modules usually work under cyclic heat stress and high current concentration, mechanical properties are also important criterias in addition to zT for TE application. Robustness of materials determines their reliability and durability during manufacturing and functioning, and to some extent, reflects the TE performance.[49] Figure 4A shows the

25673165, 2019, 1, Downloaded from https://onlinelibrary.wiley.com/doi/10.1002/inf2.12006 by Koc University, Wiley Online Library on [25/10/2026]. See the Terms and Conditions (https://onlinelibrary.wiley.com/terms-and-conditions) on Wiley Online Library for rules of use; OA articles are governed by the applicable Creative Commons License

Vicker's hardness of incorporated samples compared with some widely adopted TE materials. When C/B-NPs incorporation increases from $x = 0$ to $x = 0.45$ wt%, the hardness slightly decreases from 0.52 GPa to 0.46 GPa due to the weak stiffness of nanoinclusions. The fracture toughness of the $x = 0.10$ wt% sample shown in Figure 4B is 1.7 $MPa^{1/2}$ for α-phase and 2.1 $MPa^{1/2}$ for β-phase being comparable with pristine Cu_2Se and larger than other TE systems. This should attribute to the hardening and toughening effect from the multiscale interfaces and grain boundaries that restrict the growing and spreading of sample cracks.[50]

We also did the bending test at elevating temperatures for samples with or without C/B-NPs. From room temperature to the phase transition temperature, both samples show elastic deformation and the according amplitude remain constant. Notably, although bending is observed in both samples, the C/B-NPs incorporated sample shows less displacement, indicating that the C/B-NPs reinforce the sample's toughness against bending. For the β-phase temperature, no obvious bending can be seen for either sample. An enlargement of labelled area is shown in the inset. It is obvious that the C/B-NPs incorporated sample shows a lag with respect to the applied force, implying that nanoinclusions suppress the motion of interfaces or domains.[51] Figure 4D presents the Young's modulus measured at increasing temperature. At 450 K, the Young's modulus of the incorporated sample is 55 GPa, which is 16.7% lower than that of the pure Cu_2Se. For higher temperatures, the incorporated sample shows an increasing trend of Young's modulus, which is consistent with the increased lattice thermal conductivity shown in Figure 3E.

3 | CONCLUSION

In this work, we report the effects of carbon-coated-boron nanoparticles on the TE and mechanical properties of Cu_2Se. The incorporated samples are characterized by X-ray diffraction (XRD), scanning electron microscopy (SEM), electron backscatter diffraction (EBSD), transmission electron microscopy (TEM), electron and heat transport measurements, and mechanical properties analysis from room temperature to 1000 K. The homogeneous distribution of C/B-NPs was detected, leading to a high density of Cu:C:B interfaces. The Seebeck coefficient at 1000 K is improved from 280 μV/K for pristine Cu_2Se to 320 μV/K for 0.45 wt % C/B-NPs incorporated sample due to the energy filtering effect. Meanwhile, the lattice thermal conductivity at 1000 K is drastically reduced from 0.5 W/mK to 0.28 W/mK. Owing to the synergistic modulation of Seebeck coefficient and thermal conductivity by C/B-NPs incorporation, a significantly enhanced TE figure-of-merit of ~2.23 at 1000 K is achieved in the $x = 0.10$ wt% sample. Enhancement of the average zT and engineering zT by ~100% are also achieved owing to the high mid-temperature zT of 1.7 at 700 K. The C/B-NPs also have an evident impact on the mechanical properties of Cu_2Se, implying the competence for different manufacturing and working situations. Our work demonstrates that carbon-coated-boron is a new and effective secondary phase for Cu_2Se which can significantly enhance the zT for both mid- and high-temperatures. The ultra-high TE performance in the C/B-NPs incorporated Cu_2Se will stimulate further study and potential applications of the Cu_2Se based TE materials.

ACKNOWLEDGMENTS

This work was partially supported by the Australian Research Council (ARC) through a Discovery Project (DP 130102956, XLW), an ARC Professorial Future Fellowship project (FT 130100778, XLW), Linkage Infrastructure Equipment and Facilities (LIEF) Grant (LE 120100069, XLW), the ARC Centre of Excellence in Future Low-Energy Electronics Technologies (FLEET, CE170100039) and LIEF (LE120100104). The author thanks Dr. Mitchell Nancarrow and Dr. David Mitchell for the helpful sample characterizations.

CONFLICT OF INTEREST

The authors declare no conflict of interest.

ORCID

Umut Aydemir https://orcid.org/0000-0003-1164-1973
Xiaolin Wang https://orcid.org/0000-0003-4150-0848

REFERENCES

1. He J, Tritt TM. Advances in thermoelectric materials research: looking back and moving forward. *Science*. 2017;357(6358):eaak9997.
2. Wu HJ, Zhao LD, Zheng FS, et al. Broad temperature plateau for thermoelectric figure of merit ZT<2 in phase-separated PbTe0.7S0.3. *Nat Commun*. 2014;5:4515.
3. Liu H, Shi X, Xu F, et al. Copper ion liquid-like thermoelectrics. *Nat Mater*. 2012;11:422-425.
4. Snyder GJ, Snyder AH. Figure of merit ZT of a thermoelectric device defined from materials properties. *Energ Environ Sci*. 2017;10(11):2280-2283.
5. Snyder GJ, Toberer ES. Complex thermoelectric materials. *Nat Mater*. 2008;7:105-114.
6. Bell LE. Cooling, heating, generating power, and recovering waste heat with thermoelectric systems. *Science*. 2008;321(5895):1457-1461.
7. Zhiwei C, Xinyue Z, Yanzhong P. Manipulation of phonon transport in thermoelectrics. *Adv Mater*. 2018;30(17):1705617.
8. P-A Z, Hanus R, Dylla M, et al. Skutterudite with graphene-modified grain-boundary complexion enhances zT enabling high-efficiency thermoelectric device. *Energ Environ Sci*. 2017;10(1):183-191.

25673165, 2019, 1, Downloaded from https://onlinelibrary.wiley.com/doi/10.1002/inf2.12006 by Koc University, Wiley Online Library on [25/10/2026]. See the Terms and Conditions (https://onlinelibrary.wiley.com/terms-and-conditions) on Wiley Online Library for rules of use; OA articles are governed by the applicable Creative Commons License

9. Takabatake T, Suekuni K, Nakayama T, Kaneshita E. Phonon-glass electron-crystal thermoelectric clathrates: experiments and theory. *Rev Mod Phys*. 2014;86(2):669-716.
10. Biswas K, He J, Blum ID, et al. High-performance bulk thermoelectrics with all-scale hierarchical architectures. *Nature*. 2012; 489:414-418.
11. Thébaud S, Adessi C, Pailhès S, Bouzerar G. Boosting the power factor with resonant states: a model study. *Phys Rev B*. 2017;96 (7):075201.
12. Friedman HM, Agarwalla BK, Segal D. Effects of vibrational anharmonicity on molecular electronic conduction and thermoelectric efficiency. *J Chem Phys*. 2017;146(9):092303.
13. Mao J, Liu Z, Ren Z. Size effect in thermoelectric materials. *Npj Quantum Mater*. 2016;1:16028.
14. Chang C, Wu M, He D, et al. 3D charge and 2D phonon transports leading to high out-of-plane *ZT* in n-type SnSe crystals. *Science*. 2018;360(6390):778-783.
15. Zhao L-D, Lo S-H, Zhang Y, et al. Ultralow thermal conductivity and high thermoelectric figure of merit in SnSe crystals. *Nature*. 2014;508:373-377.
16. Tan G, Shi F, Hao S, et al. Non-equilibrium processing leads to record high thermoelectric figure of merit in PbTe–SrTe. *Nat Commun*. 2016;7:12167.
17. Heremans JP, Jovovic V, Toberer ES, et al. Enhancement of thermoelectric efficiency in PbTe by distortion of the electronic density of states. *Science*. 2008;321(5888):554-557.
18. Zybała R, Schmidt M, Kamińska P, et al. Skutterudite (CoSb3) thermoelectric nanomaterials fabricated by pulse plasma in liquid. *Mater Today: Proc*. 2018;5(4, Part 1):10316-10322.
19. Hong M, Wang Y, Feng T, et al. Strong phonon-phonon interactions securing extraordinary thermoelectric $Ge_{1-x}Sb_xTe$ with Zn-alloying-induced band alignment. *J Am Chem Soc*. 2019;141(4): 1742-1748.
20. Tritt TM, Subramanian MA. Thermoelectric materials, phenomena, and applications: a bird's eye view. *MRS Bullet*. 2006;31(3):188-198.
21. Chen Z-G, Shi X, Zhao L-D, Zou J. High-performance SnSe thermoelectric materials: progress and future challenge. *Prog Mater Sci*. 2018;97:283-346.
22. Goldsmid HJ. *Introduction to Thermoelectricity*. Vol 1. Berlin Heidelberg: Springer Series in Material Science; 2010.
23. Tiejun Z, Yintu L, Chenguang F, P. HJ, G. SJ, Xinbing Z. Compromise and synergy in high-efficiency thermoelectric materials. *Adv Mater*. 2017;29(14):1605884.
24. Lee M-J, Ahn J-H, Sung JH, et al. Thermoelectric materials by using two-dimensional materials with negative correlation between electrical and thermal conductivity. *Nat Commun*. 2016; 7:12011.
25. Xiao C, Li Z, Li K, Huang P, Xie Y. Decoupling interrelated parameters for designing high performance thermoelectric materials. *Acc Chem Res*. 2014;47(4):1287-1295.
26. Wang H, Pei Y, LaLonde AD, Snyder GJ. Weak electron–phonon coupling contributing to high thermoelectric performance in n-type PbSe. *Proc Natl Acad Sci*. 2012;109(25):9705-9709.
27. Kim HS, Liu W, Chen G, Chu C-W, Ren Z. Relationship between thermoelectric figure of merit and energy conversion efficiency. *Proc Natl Acad Sci U S A*. 2015;112(27):8205-8210.
28. He R, Kraemer D, Mao J, et al. Achieving high power factor and output power density in p-type half-Heuslers $Nb_{1-x}Ti_xFeSb$. *Proc Natl Acad Sci*. 2016;113(48):13576-13581.
29. Banik A, Shenoy US, Saha S, Waghmare UV, Biswas K. High power factor and enhanced thermoelectric performance of SnTe-AgInTe2: synergistic effect of resonance level and valence band convergence. *J Am Chem Soc*. 2016;138(39):13068-13075.
30. Shuai J, Mao J, Song S, et al. Tuning the carrier scattering mechanism to effectively improve the thermoelectric properties. *Energ Environ Sci*. 2017;10(3):799-807.
31. Yanzhong P, Heng W, Snyder GJ. Band engineering of thermoelectric materials. *Adv Mater*. 2012;24(46):6125-6135.
32. He J, Kanatzidis MG, Dravid VP. High performance bulk thermoelectrics via a panoscopic approach. *Mater Today*. 2013;16 (5):166-176.
33. Peng K, Lu X, Zhan H, et al. Broad temperature plateau for high ZTs in heavily doped p-type SnSe single crystals. *Energ Environ Sci*. 2016;9(2):454-460.
34. Zhao L, Islam SMKN, Wang J, et al. Significant enhancement of figure-of-merit in carbon-reinforced Cu2Se nanocrystalline solids. *Nano Energy*. 2017;41:164-171.
35. Nunna R, Qiu P, Yin M, et al. Ultrahigh thermoelectric performance in Cu2Se-based hybrid materials with highly dispersed molecular CNTs. *Energ Environ Sci*. 2017;10(9):1928-1935.
36. Tang H, Sun F-H, Dong J-F, et al. Graphene network in copper sulfide leading to enhanced thermoelectric properties and thermal stability. *Nano Energy*. 2018;49:267-273.
37. Jang JI, Lee JE, Kim B-S, Park S-D, Lee HS. Twinning and its formation mechanism in a binary Mg2Si thermoelectric material with an anti-fluorite structure. *RSC Adv*. 2017;7(35):21671-21677.
38. Mao J, Wang Y, Kim HS, et al. High thermoelectric power factor in cu–Ni alloy originate from potential barrier scattering of twin boundaries. *Nano Energy*. 2015;17:279-289.
39. Chu F, Zhang Q, Zhou Z, Hou D, Wang L, Jiang W. Enhanced thermoelectric and mechanical properties of Na-doped polycrystalline SnSe thermoelectric materials via CNTs dispersion. *J Alloys Compd*. 2018;741:756-764.
40. Kim H-S, Gibbs ZM, Tang Y, Wang H, Snyder GJ. Characterization of Lorenz nnumber with seebeck ccoefficient mmeasurement. *APL Mater*. 2015;3(4):041506.
41. Liu R, Chen H, Zhao K, et al. Entropy as a gene-like performance indicator promoting thermoelectric materials. *Adv Mater*. 2017;29 (38):1702712.
42. Slack GA. The thermal conductivity of nonmetallic crystals. In: Ehrenreich H, Seitz F, Turnbull D, eds. *Solid State Physics*. Vol 34. Amsterdam: Academic Press; 1979:1-71.
43. Li G, Gadelrab KR, Souier T, Potapov PL, Chen G, Chiesa M. Mechanical properties of bi x Sb 2− x Te 3 nanostructured thermoelectric material. *Nanotechnology*. 2012;23(6):065703.
44. Ren F, Case ED, Timm EJ, Lara-Curzio E, Trejo RM. Anomalous temperature-dependent Young's modulus of a cast LAST (Pb–Sb–Ag–Te) thermoelectric material. *Acta Mater*. 2010;58(1):31-38.
45. Ren F, Case ED, Ni JE, et al. Temperature-dependent elastic moduli of lead telluride-based thermoelectric materials. *Philos Mag*. 2009;89(2):143-167.
46. Pei Y, Chang C, Wang Z, et al. Multiple converged conduction bands in K2Bi8Se13: a promising thermoelectric material with extremely low thermal conductivity. *J Am Chem Soc*. 2016;138 (50):16364-16371.
47. Pei Y-L, He J, Li J-F, et al. High thermoelectric performance of oxyselenides: intrinsically low thermal conductivity of Ca-doped BiCuSeO. *Npg Asia Mater*. 2013;5:e47.

25673165, 2019, 1, Downloaded from https://onlinelibrary.wiley.com/doi/10.1002/inf2.12006 by Koc University, Wiley Online Library on [25/10/2026]. See the Terms and Conditions (https://onlinelibrary.wiley.com/terms-and-conditions) on Wiley Online Library for rules of use; OA articles are governed by the applicable Creative Commons License

48. Sanditov DS, Belomestnykh VN. Relation between the parameters of the elasticity theory and averaged bulk modulus of solids. *Tech Phys*. 2011;56(11):1619-1623.
49. Liu Z, Mao J, Sui J, Ren Z. High thermoelectric performance of α-MgAgSb for power generation. *Energ Environ Sci*. 2018;11(1): 23-44.
50. Lee S-C, Ho W-Y. The effects of surface hardening on fracture toughness of carburized steel. *Metallurg Trans A*. 1989;20(3): 519-525.
51. Ye JC, Lu J, Liu CT, Wang Q, Yang Y. Atomistic free-volume zones and inelastic deformation of metallic glasses. *Nat Mater*. 2010;9:619-623.

SUPPORTING INFORMATION

Additional supporting information may be found online in the Supporting Information section at the end of this article.

How to cite this article: Li M, Islam Sheik Md. Kazi Nazrul, Yahyaoglu M, et al. Ultrahigh figure-of-merit of Cu_2Se incorporated with carbon coated boron nanoparticles. *InfoMat*. 2019;1:108–115. https://doi.org/10.1002/inf2.12006

25673165, 2019, 1, Downloaded from https://onlinelibrary.wiley.com/doi/10.1002/inf2.12006 by Koc University, Wiley Online Library on [25/10/2026]. See the Terms and Conditions (https://onlinelibrary.wiley.com/terms-and-conditions) on Wiley Online Library for rules of use; OA articles are governed by the applicable Creative Commons License